An innovative sensor for hydroxylamine determination: Using molybdenum hybrid zeolitic imidazolate framework–conducting polymer composite as electrocatalyst

Cuiyuan Liang [a], Feng Zhang [a, *], Huiming Lin [a], Cheng Jiang [c], Wei Guo [a], Songjie Fan [b], Fengyu Qu [a, **]

[a] Key Laboratory of Photochemical Biomaterials and Energy Storage Materials, Heilongjiang Province and College of Chemistry and Chemical Engineering, Harbin Normal University, Harbin, 150025, PR China
[b] Research Institute of Medicine and Pharmacy, Qiqihar Medical University, Qiqihar, 161006, PR China
[c] School of Chemistry and Materials Science, Nanjing Normal University, Nanjing, 210023, PR China

ARTICLE INFO

ABSTRACT

A novel composite material, hybrid zeolitic imidazolate framework (HZIF)–conducting poly(3,4-ethylenedioxythiophene) (PEDOT) has been fabricated on carbon cloth electrode (CCE) by microwave-assisted crystallization, followed by drop-coating and vapor deposition procedures. Specifically, the HZIF inserted by molybdenum (HZIF-Mo) is entitled to intrinsic catalytic activity towards amine molecules, which is firstly integrated with the conductive and catalytic PEDOT as an enhanced electrochemical sensor for hydroxylamine. Detection is performed by amperometric method, and the composite sensor (HZIF-Mo/PEDOT/CCE) shows a low detection limit of $0.04 \, \mu M \, (S/N = 3)$ in the linear range of $0.1-692.2$ μM, along with superior anti-interference ability, reproducibility (RSD = 4.43%) and outstanding performance in real samples. As noticed, the hydroxylamine catalytic process combines the advantages of the alkaline-stable HZIF-Mo containing ample catalytic sites and high surface area and the mesoporous PEDOT reining in outstanding conductivity and redox capability, thereby imparting amplified electrochemical signals. This work undertakes an opening to expand MOF-based composites for versatile sensing applications.

© 2019 Elsevier Ltd. All rights reserved.

1. Introduction

Hydroxylamine which is derivative of ammonia is mainly used as reducing and imaging agents in life [1,2]. However, its exceeding toxicity can arouse damage to aquatic organisms, and stimulate mutagenesis on the respiratory system and skin, even at moderate levels. Moreover, hydroxylamine can strongly decompose due to its extremely impoverished stability, and then generates toxic oxides when exposure to oxidizing substances [3]. Consequently, it is exceptionally meaningful to connect advanced materials with the assist of doubtless detection techniques (e.g., electrochemical strategy) to sensitively monitor hydroxylamine.

Lately, metal-organic frameworks (MOFs), a newfangled class of crystalline materials, have emerged wide-ranging attentions not only for their attractive features (e.g., tunable structures, rich porosities and high internal surface areas) but also for underlying applications in electrochemical territory (e.g., energetic storage, electrocatalysis and undiscovered electrocatalytic composites) [4,5]. Nevertheless, the aforesaid applications from multifold MOFs are restricted by their inherent stabilities under severe surroundings and limited electrocatalytic activities [6]. Deservedly, a classic type of MOFs, zeolitic-imidazolate frameworks (ZIFs) consisting of metallic nodes (e.g., Zn^{2+} and Co^{2+}) bridged by imidazole linkers, have caused great interests arising from unique characteristics, such as permanent porosities coupled with excellent chemical/thermal stabilities (>550 °C under N_2 atmosphere) referring to other MOFs [7]. Meanwhile, hybrid ZIFs (HZIFs) walk into the researchers' vision, which simultaneously unify compositional and structural merits of ZIFs and zeolites, inserting TO_4 tetrahedra ($T = Mo^{6+}$ or W^{6+}) with metal-imidazolate components. Moreover, introducing

redox-active heteroatom units (TO$_4$) into ZIFs can immensely expand HZIFs on electrochemical application [8–10]. Nevertheless, different than ZIFs in battery and supercapacitor [11,12], only several ZIFs (e.g., ZIF-8 [13–15] and ZIF-67 [16,17]) have been enlarged as electrochemical detectors, and revolved around functionalized frameworks/composites to boost selectivity or sensitivity for glucose/H$_2$O$_2$ molecules [18–22]. Hereunto, to our survey, the sparse attention has been paid on ZIFs to detect hydroxylamine, and further, there is no previous example that employs HZIFs as electrochemical sensors, although incorporating electroactive oxide blocks in HZIFs can accelerate the electrocatalytic activity.

In this work, we strived to an impressive hybrid zeolitic imidazolate framework [Zn$_4$(im)$_6$MoO$_4$] (denoted as HZIF-Mo, im: 2-methylimidazolate) for amperometric sensor towards hydroxylamine. Markedly, the Zn(im)$_4$/ZnN$_4$ unit inside ZIF-8 substitutes with MoO$_4$ blocks in HZIF-Mo with high thermal stability [23]. More importantly, the incorporation of catalytically active heteroatoms provides a consummate support for electrochemical detection [24–26]. Meanwhile, a conducting poly(3,4-ethylenedioxythiophene) (PEDOT) is merged with HZIF-Mo (HZIF-Mo/PEDOT), which can figure out the limitation of frangible electrical conductivity and hydrophobic behavior of ZIFs [27]. Preferably, PEDOT is utilized as polymeric matrix due to its environmental compatibility; also, the admirable conductivity of PEDOT (up to 4500 σ cm^{-1} during vapor deposition [28,29]) can quicken electron/ion diffusion, and thus availably strengthen the conductivity of HZIF-Mo/PEDOT composite. If the detection line and sensitivity towards target molecule can be further improved by confident composite means, this alternative sensing material (HZIF-Mo) will have unexceptionable application potential. Herein, the high crystallization of alkaline-stable HZIF-Mo is obtained for the first time by microwave-assisted technique, which is blended with conductive PEDOT supported on carbon cloth electrode (HZIF-Mo/PEDOT/CCE) for hydroxylamine detection, followed by drop-coating and vapor deposition procedures (Scheme 1). The developed complex sensor possesses the mounting active sites, the augmented effective active areas together with the improved conductivity comparison to single MOF and PEDOT based catalysts. These respects are ultimately responsible for HZIF-Mo/PEDOT/CCE electrode to acquire exceptional detection performance towards hydroxylamine including detection line (0.04 μM), anti-interference ability and recovery in real samples.

2. Experimental section

2.1. Reagents and instruments

Zinc acetate dihydrate (Zn(CH$_3$COO)$_2$·2H$_2$O, ≥99%), chloride hexahydrate (FeCl$_3$·6H$_2$O, ≥99%), 2-methylimidazole (2-Mim, ≥99%), 3,4-ethylenedioxythiophene (EDOT, ≥99%), molybdic acid (H$_2$MoO$_4$, ≥99%) and hydroxylamine (NH$_2$OH·HCl, ≥98.5%) were bought from Acros organics Company. N, N-dimethylformamide (DMF, ≥99%), ethanol (C$_2$H$_5$OH, ≥99%) were purchased from Tianjin Fuyu Fine Chemical Co. Ltd. All reagents were used directly without further purification. Carbon cloth electrodes (CCE) were purchased from Taiwan Ce Tech Co., Ltd.
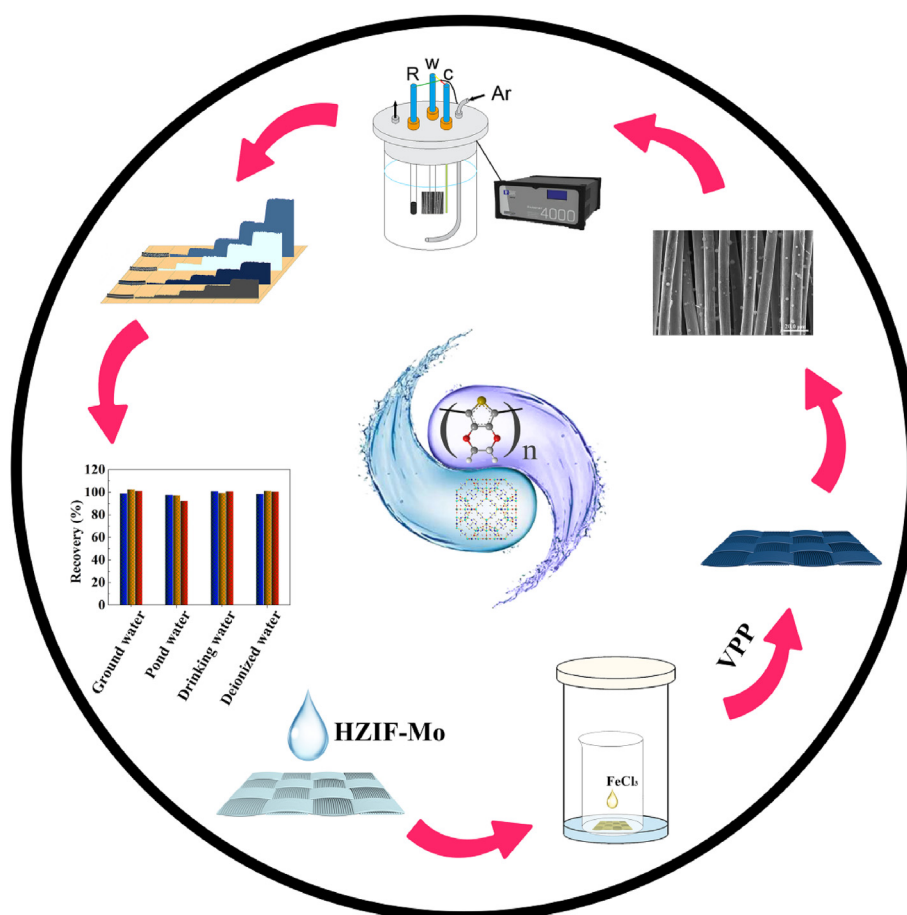
Scheme 1. Schematic representation of the fabrication process of HZIF-Mo/PEDOT/CCE.

Powder X-ray diffraction (PXRD) patterns were gained on a Rigaku Ultima IV X-ray diffractometer with Cu-K$_\alpha$ radiation ($\lambda = 1.5420$ Å) under 40 kV and 30 mA. Fourier transform infrared (FT-IR) spectra were performed in the range 400−4000 cm^{-1} using a Bruker Tensor II spectrometer. The field-emission scanning electron microscopy (SEM) images were measured on a Hitachi S-4800 microscope and energy dispersive spectrometry (EDS) analyses were performed on a Hitachi SU-70 scanning electron microscope. The nitrogen adsorption-desorption isotherms were obtained on an autosorb iQ2 instrument (Quantachrome U.S.) at 77 K after samples were pretreated at 393 K for 12 h. Raman spectra were covered on a LabRAM HR800 system using 488 nm lasers (Horiba, France). Thermogravimetric analyses (TGA) were implemented on a Mettler-Toledo TGA analyzer under an air atmosphere at a heating rate of 10 K min^{-1}.

2.2. Preparation of HZIF-Mo by microwave-assisted method

HZIF-Mo was synthesized as follows: Zn(CH$_3$COO)$_2$·2H$_2$O (0.8800 g, 0.40 mmol), H$_2$MoO$_4$ (0.0162 g, 0.10 mmol) and 2-Mim (0.0480 g, 0.585 mmol) were successively slotted in a beaker containing DMF (4.0 mL), and stirred at room temperature until the reactants dissolved. Afterwards, the suspension was poured into a microwave reactor and heated at varied temperatures (333 and 393 K) and time (60−600 s) (Intelligent Microwave System, Xintuo Analytical Instruments, Shanghai, China). The solid obtained was centrifuged using water and ethanol, respectively, in five subsequent cycles (8000 r min^{-1}), and dried overnight at 373 K under vacuum.

2.3. Fabrication of HZIF-Mo/PEDOT/CCE

Prior to fabrication of HZIF-Mo/PEDOT/CCE composite electrodes, CCEs (10 × 10 mm^2 size) were placed in acetone and deionized water under ultrasound for 15 min, respectively, and then boiled in concentrated nitric acid at 363 K for 4 h. Afterwards, CCEs were repeatedly cleaned with deionized water and ethanol until neutral, and dried at 343 K.

A HZIF-Mo/PEDOT/CCE was prepared by drop-coating and vapor phase polymerization (VPP) process (Scheme 1). In a typical process, HZIF-Mo was ultrasonically dispersed in ethanol under a frequency of 20 kHz for 30 min to obtain a homogenous dispersion (1.0 mg mL^{-1}). The dispersion (30 μL) was dropped on a bare CCE, and then allowed to air dry (HZIF-Mo/CCE). Subsequently, FeCl$_3$ solution (0.50 M, 5.0 μL) was spread over HZIF-Mo/CCE, and placed in an EDOT deposition reactor to polymerize EDOT at 403 K for 1 h. The obtained composite (HZIF-Mo/PEDOT/CCE) was washed with mass of distilled water and ethanol, respectively, and dried in air for further use.

2.4. Electrochemical measurements

A three-electrode electrochemical cell was employed for electrochemical studies on a PARSTAT 4000 electrochemical analyzer (Princeton Applied Research, USA). Platinum wire and saturated calomel electrode (SCE) were used as the counter and reference electrodes, respectively. The working electrodes were HZIF-Mo/ PEDOT/CCE as well as CCE, HZIF-Mo/CCE and PEDOT/CCE for comparison. Nitrogen purging of 0.1 M phosphate buffer (pH 9.0) was used as electrolyte. Electrical impedance spectroscopy (EIS) were recorded from 0.1 to 10 kHz for in 0.1 mM KCl solution containing 0.5 mM Fe(CN)$_6^{3-/4-}$.

3. Results and discussion

3.1. Characterization of HZIF-Mo and composites

Powder X-ray diffraction (PXRD) patterns of HZIF-Mo by microwave-assisted strategy under different crystallization temperature and time are shown in Fig. S1. From PXRD patterns, the crystal structure of HZIF-Mo obtained by microwave-assisted heat is almost consistent with that of the simulated one, suggesting that HZIF-Mo is successfully synthesized. More importantly, the smaller size HZIF-Mo than that by the conventional electric heating is liable to firmly attach onto CCEs, which contributes to steadily electrocatalytic detection. Finally, HZIF-Mo synthesized at 393 K and 300 s is selected for the sequential experiments.

The structure of HZIF-Mo/PEDOT/CCE is also performed using PXRD analysis. As apparent in Fig. 1, the pristine CCE and PEDOT are displayed broad diffraction peaks at about 25.56° [30] and 24.91° ((020) reflection) [31,32], respectively, indicating the typically amorphous or low crystallinity. When HZIF-Mo dripped onto CCE, the characteristic peaks of the ZIF obviously appear in the PXRD patterns of HZIF-Mo/CCE composite. While, there is obvious diffraction peak in CCE modified by HZIF-Mo/PEDOT (0.12 mg cm^{-2}). Therefore, it is speculated that HZIF-Mo and PEDOT have been blended onto CCE matrix.

The morphological features of PEDOT/CCE, HZIF-Mo/CCE and HZIF-Mo/PEDOT/CCE were compared by SEM images (Figs. 2 and S2). PEDOT/CCE covers the CCE surface, evenly as cotton batting (Fig. 2a and b). The CCE also adheres to HZIF-Mo, which is a regular and polyhedron (Fig. 2c and d). Moreover, it can be distinctly seen that a conductive PEDOT and redox capable HZIF-Mo simultaneously leech on to the CCE surface, as depicted in Fig. 2e and f , which identifies with the elemental mapping analyses of HZIF-Mo/ PEDOT/CCE (Fig. 2g). This tight gathering provides a favorable support for the electrochemical detection of hydroxylamine.

The combination of HZIF-Mo and PEDOT is also validated by FT-IR and Raman spectra (Fig. 3a and b). The C−H stretching (3136 cm^{-1}), methyl group (2923 cm^{-1}) and plane bending (1303, 1143 and 758 cm^{-1}) in the imidazole ring emerge on the FT-IR spectrum of HZIF-Mo/PEDOT composite; meanwhile, the peaks corresponding to C−S−C vibration from the thiophene ring are also
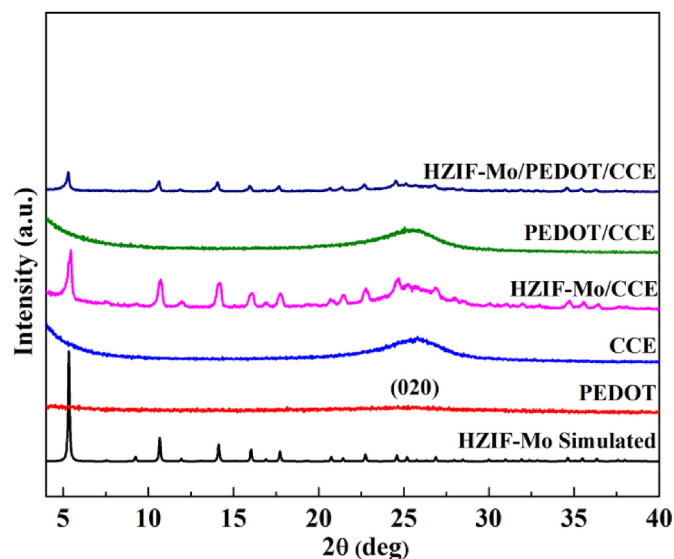

Fig. 1. PXRD patterns of the simulated HZIF-Mo, PEDOT, CCE, HZIF-Mo/CCE, PEDOT/CCE and HZIF-Mo/PEDOT/CCE.
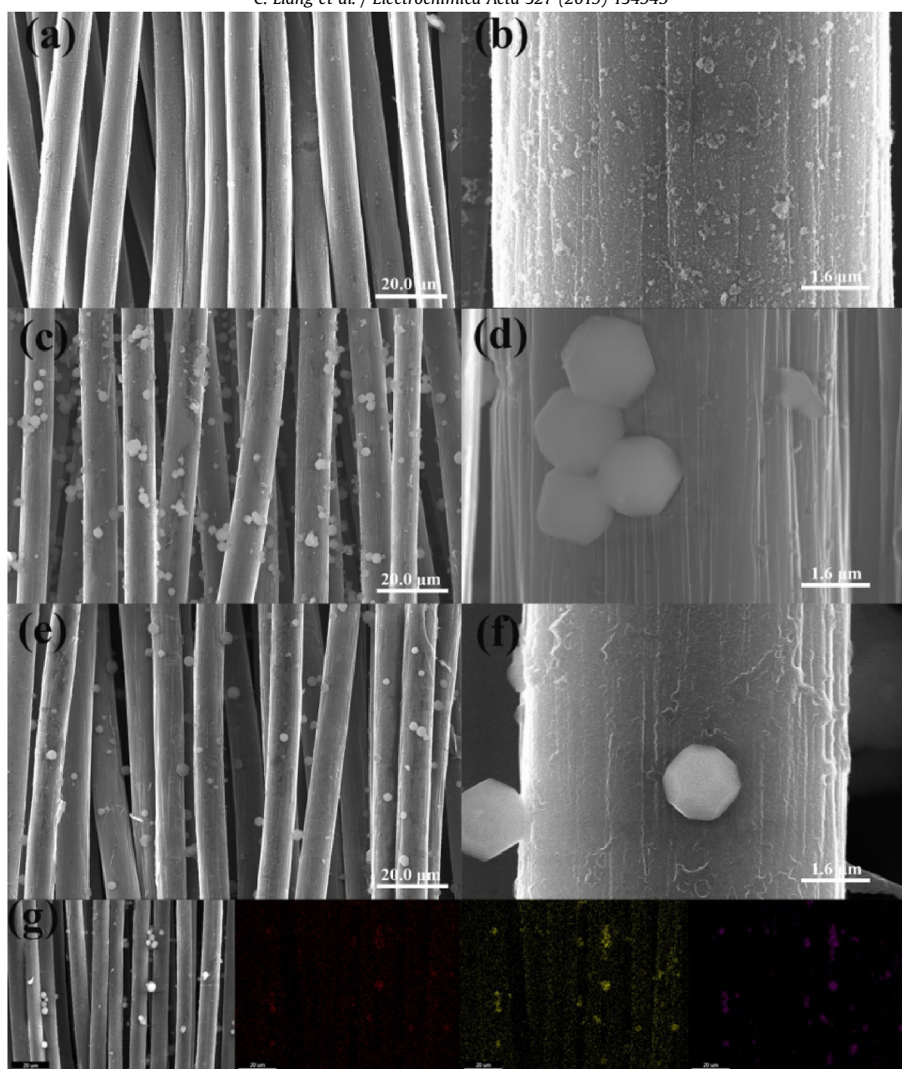
Fig. 2. SEM images of (a and b) PEDOT/CCE, (c and d) HZIF-Mo/CCE and (e and f) HZIF-Mo/PEDOT/CCE; (g) elemental mapping images of HZIF-Mo/PEDOT/CCE.

observed at 986 and 692 cm^{-1} [33,34]. We also monitored the stretching vibration of C=C (1477 cm^{-1}) and inter-ring stretching mode of C−C (1355 cm^{-1}) stemmed from PEDOT in the infrared spectrum of HZIF-Mo/PEDOT. Additionally, the composite exhibits the significant and slightly widened bands at 896 (Mo−O) and 423 cm^{-1} (Zn−N) comparison to HZIF-Mo [35]; the bending vibration of C−O−C (1236 and 1063 cm^{-1}) in the ethylenedioxy group are slightly wider than that of pristine PEDOT; the slight red shift of 986 cm^{-1} may be pinned on the mutual binding force of HZIF-Mo. Raman bands in PEDOT at 1445 and 1501 cm^{-1} belong to the symmetric stretching vibration of $C_{\alpha} = C_{\beta}$ (-O) and the asymmetric stretching of $C_{\alpha} = C_{\beta}$, which also present in HZIF-Mo/PEDOT composites [36,37] (Fig. 3b). Thus, HZIF-Mo is successfully combined with PEDOT, and exists the interaction between them.

Thermal gravimetric analysis (TGA) is a fundamental method to inspect the thermal stability of materials. As displayed in Fig. 3c, there is a loss for HZIF-Mo after ~380 °C, possibly attributed to the framework decomposition. PEDOT decorated HZIF-Mo can be stable up to about ~310 °C [38]. Further, HZIF-Mo has admirable stability under alkaline conditions (Fig. S3).

The porosities of HZIF-Mo, PEDOT and its composite were investigated by nitrogen sorption, as displayed in Fig. 3d. The Brunauer-Emmet-Teller surface area (S_{BET}) of HZIF-Mo/PEDOT drops to 308.94 m^2 g^{-1}, comparison to that of HZIF-Mo ($S_{BET} =$

452.66 m^2 g^{-1}) [23]. After HZIF-Mo combined with PEDOT, the pore size of ZIF decreases to 8.52 Å, and a range of 20−40 Å ascribes to that of PEDOT (Fig. S4 and Table S1). These results indicate that HZIF-Mo/PEDOT is tantamount to the backbone for PEDOT, and confers a high surface area and more electroactive sites (MoO$_4$ units).

3.2. Electrochemical detection of hydroxylamine

3.2.1. Electrochemical behavior of the modifed electrodes

The electrochemical impedance spectroscopy (EIS) is usually adapted to dissect the interface electron transfer between different electrodes. As seen from EIS, the resistance of HZIF-Mo/CCE (0.43 kΩ) basically is in line with the result of bare CCE (0.42 kΩ) (Fig. 4a). For HZIF-Mo/PEDOT/CCE, its electron transfer resistance obviously decreases to 0.35 kΩ (Fig. 4b), profiting from high conductivity of PEDOT [39].

The electrochemical properties of four electrodes are investigated by cyclic voltammograms (CVs) in 0.1 M PBS (pH 9.0) without and with 0.5 mM hydroxylamine, respectively (Fig. 4c and d). It can be found that these electrodes have different levels of response to hydroxylamine. Regarding Fig. 4c, the bare CCE only shows a weak response to hydroxylamine oxidation (0.56 mA cm^{-2}); whereas the CCE modified with PEDOT exhibits a single observable peaks at
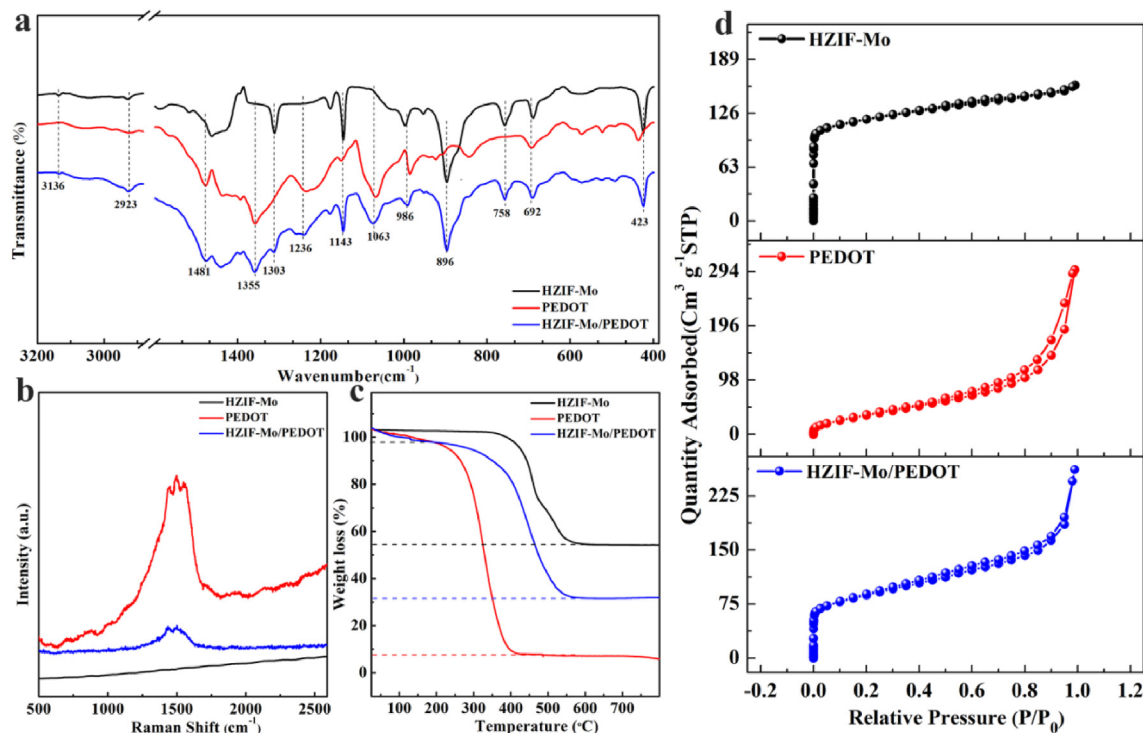
Fig. 3. (a) FT-IR spectra, (b) Raman spectra, (c) TGA and (d) N_2 adsorption-desorption isotherms of HZIF-Mo, PEDOT and HZIF-Mo/PEDOT.

0.82 V (1.12 mA cm^{-2}). The existence of conductive PEDOT is more favorable for the oxidation of hydroxylamine specie [40]. Further, the peak current of hydroxylamine at HZIF-Mo/CCE (1.32 mA cm^{-2}) is 2.36 and 1.18-fold increases than those of CCE and PEDOT/CCE, respectively. Also, there is a visible promotion in the current response when CCE modified by HZIF-Mo/PEDOT (1.88 mA cm^{-2}). This response enlargement is possibly ascribed to the high electroconductibility, electrocatalytic action and synergistic effect of HZIF-Mo, PEDOT and CCE, which afford the high-current detection of hydroxylamine. Additionally, the comparative probes of CCEs modified electrodes towards hydroxylamine oxidation are further identified by amperometry. Fig. 4f depicts the typical current time dynamic response (i−t) of these electrodes towards successively adding hydroxylamine from 1.0 to 7.0 μM in PBS (pH 9.0). Clearly, the response current of CCE, PEDOT/CCE, HZIF-Mo/CCE and HZIF-Mo/PEDOT/CCE forwards with an increase concentration of hydroxylamine, and their responses attain 95% of the steady-state current beneath 5 s. It can be also found that the HZIF-Mo/ PEDOT/CCE composite is more sensitive to detect hydroxylamine.

The effective areas (EAs) of CCE modified electrodes are calculated from the Randles-Sevcik reversible equation by CV technique:

$$I_p = 269\,An^{3/2}D^{1/2}\,CV^{1/2} \tag{1}$$

where A, n, D and C represent the electrode area (cm^2), the charge number that joins in electrochemical process, the diffusion coefficient of [Fe(CN)$_6$]$^{3-/4-}$ [41] and the electrolytic concentration (mol L^{-1}), respectively. Regarding Fig. S8, the EA of HZIF-Mo/PEDOT/CCE (21.59 cm^{-2}) is higher than those of the bare CCE (3.19 cm^{-2}), HZIF-Mo/CCE (10.81 cm^{-2}) and PEDOT/CCE (14.93 cm^{-2}), calculated from the slope of I$_p$ versus $v^{1/2}$ (Table S2). The enhancement of EA on the HZIF-Mo/PEDOT/CCE can extend the reaction sites and amplify the current response, thereby improving the sensitivity of hydroxylamine detection.

The reaction kinetic of hydroxylamine oxidation at HZIF-Mo/

PEDOT/CCE composite is further investigated by CV measurements under different scans. As observed from Fig. 5, the peak potential (E$_p$) and the peak current (I$_p$) slightly shift following an increase of scan rate (v). The E$_p$ and I$_p$ are proportional to the nature logarithm of scan rate (ln$v$) and square root of the scan rate ($v^{1/2}$), respectively (Fig. 5b and c), proving that the electrocatalytic reaction of hydroxylamine follows the irreversible and diffusion controlled process. Further, the rate limiting step is a single electron transfer process judged by the average value for αn_α 0.22, (α: the electron transfer coefficient, n$_\alpha$: the electron number) according to Equation (2). The Randles-Sevcik non-reversible equation (Eq. (3)) is used to calculate the total number of electrons (n) in the hydroxylamine oxidation.

$$E_p - E_{p/2} = 1.857RT\big/an_aF = 0.0477\big/an_a \tag{2}$$

$$I_p = \left(0.4958 \times 10^{-3}\right)nF^{3/2}(RT)^{-1/2}(an_a)^{1/2}AcD^{1/2}v^{1/2} \tag{3}$$

where D is the diffusion coefficient of 6.8×10^{-6} cm^2 S^{-1} (double potential step chronocoulometry studies, DPSC) [42,43] and E$_{p/2}$ is the potential corresponding to I$_{p/2}$. Thus, the n value is roughly equal to 2.3. The oxidation process of the total number of electrons electrode towards hydroxylamine can be estimated as $2NH_2OH \rightarrow N_2O + H_2O^+ \ 4H^+ + 4e^-$ [44,45]:

To elucidate different signal enhancement abilities of CCE modified electrodes, the adsorption capacity and diffusion coefficient of electrodes are measured by DPSC technique (Fig. S9).

$$Q = 2nFACD^{1/2}\pi^{-1/2}\,t^{1/2} + Q_{dl} + Q_{ads} \tag{4}$$

According to Anson formula [46], Q$_{dl}$ and Q$_{ads}$ (Q$_{ads}$ = nFAΓ_s) stand for the charge quantity of electric double layer and the Faradaic charge, respectively (Equation (4)); Γ_s is the quantity of electrolyte active species adsorbed on electrode surface. As attested
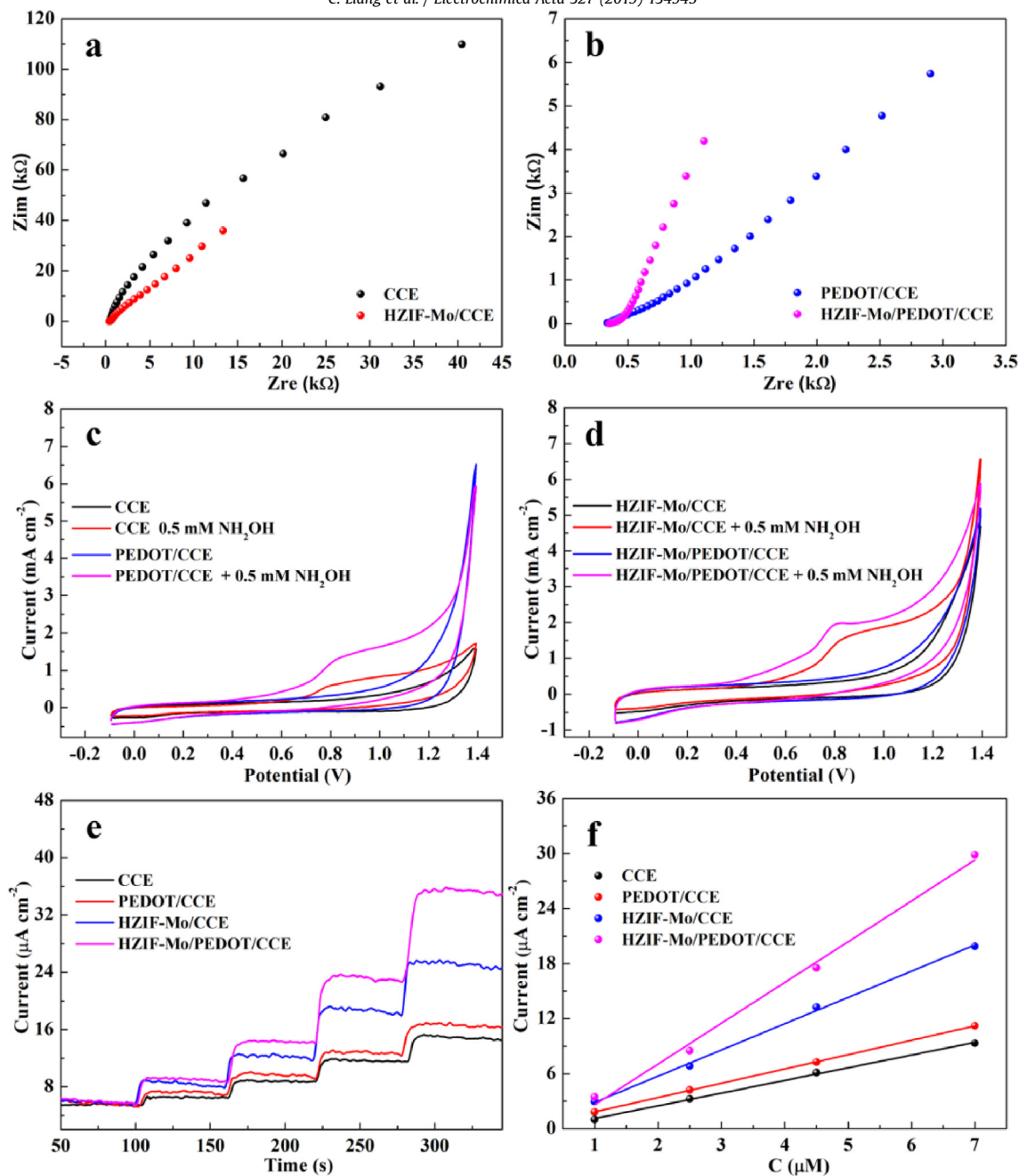
Fig. 4. EIS of (a) CCE and HZIF-Mo/CCE, (b) PEDOT/CCE and HZIF-Mo/PEDOT/CCE composites; CVs of (c) CCE and PEDOT/CCE, (d) HZIF-Mo/CCE and HZIF-Mo/PEDOT/CCE at 50 mV s^{-1} without and with hydroxylamine, respectively; (e) the amperometric response to CCE, PEDOT/CCE, HZIF-Mo/CCE, and HZIF-Mo/PEDOT/CCE in the presence of hydroxylamine applied a potential of 0.7 V; (f) the corresponding linear plots of current response *versus* hydroxylamine concentration.

by Cottrell theory [47], the intercept of $Q_f - t^{1/2}$ (0.25−0.50 V) includes Q_{dl} and Q_{ads}, and that of $Q_r - f(t)$ (0.50−0.25 V) consists of only Q_{dl} (Fig. 6). Thus, the adsorption capacity (Γ_s) and diffusion coefficient (D) of these electrodes can be calculated (Table S3). The Γ_s value of hydroxylamine at HZIF-Mo/PEDOT/CCE is 1.77×10^{-11} mol cm^{-2}, which is obviously higher than that of HZIF-Mo/CCE. Additionally, the rationality of diffusion coefficient (2.46×10^{-6} cm^2 S^{-1}) in the HZIF-Mo/PEDOT/CCE is verified by different methods (scan rates and DPSC), tying in with the assumed order of magnitude (6.8×10^{-6} cm^2 S^{-1}). The relatively high adsorption capacity and diffusion coefficient imply that the integration of PEDOT and HZIF-Mo makes the composite electrode effectively accumulate hydroxylamine on the surface.

3.2.2. Optimization of detective conditions

The testing performance of the sensor is influenced by pH, working potential, and the amount of HZIF-Mo and PEDOT onto CCEs. Undoubtedly, hydroxylamine has two forms of aprotic NH$_2$OH and protonated NH$_3$OH$^+$ in solution [48,49], suggesting that its oxidation is strongly related to pH. Therefore, cyclic voltammograms (CVs) of hydroxylamine for HZIF-Mo/PEDOT/CCE is acquainted to explore pH effect (from 7.5 to 9.5) in PBS solution. The maximum response is reached at pH 9.0, and then decreases with a further increase of pH (Fig. S7a), resulting from the instability of hydroxylamine at high pH values. Additionally, the effect of polymerized time of EDOT and the amount of HZIF-Mo are investigated by the amperometric method. The relatively prominent deposition
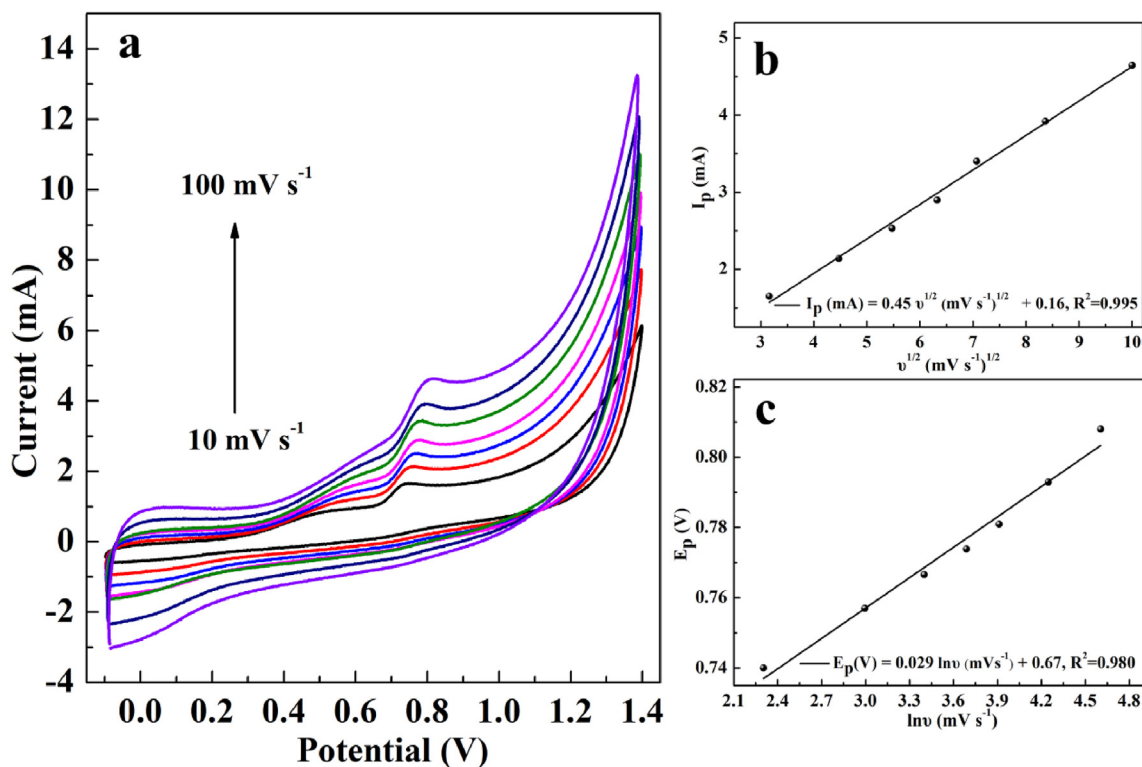
Fig. 5. (a) CVs of HZIF-Mo/PEDOT/CCE at different scan rates (*from inner to outer:* 10, 20, 30, 40, 50, 70 and 100 mV s^{-1}) of 0.8 mM hydroxylamine at PBS solution (pH 9.0); the plots of (b) I$_p$ current *versus* $v^{1/2}$ and (c) E$_p$ *versus* ln$v$.
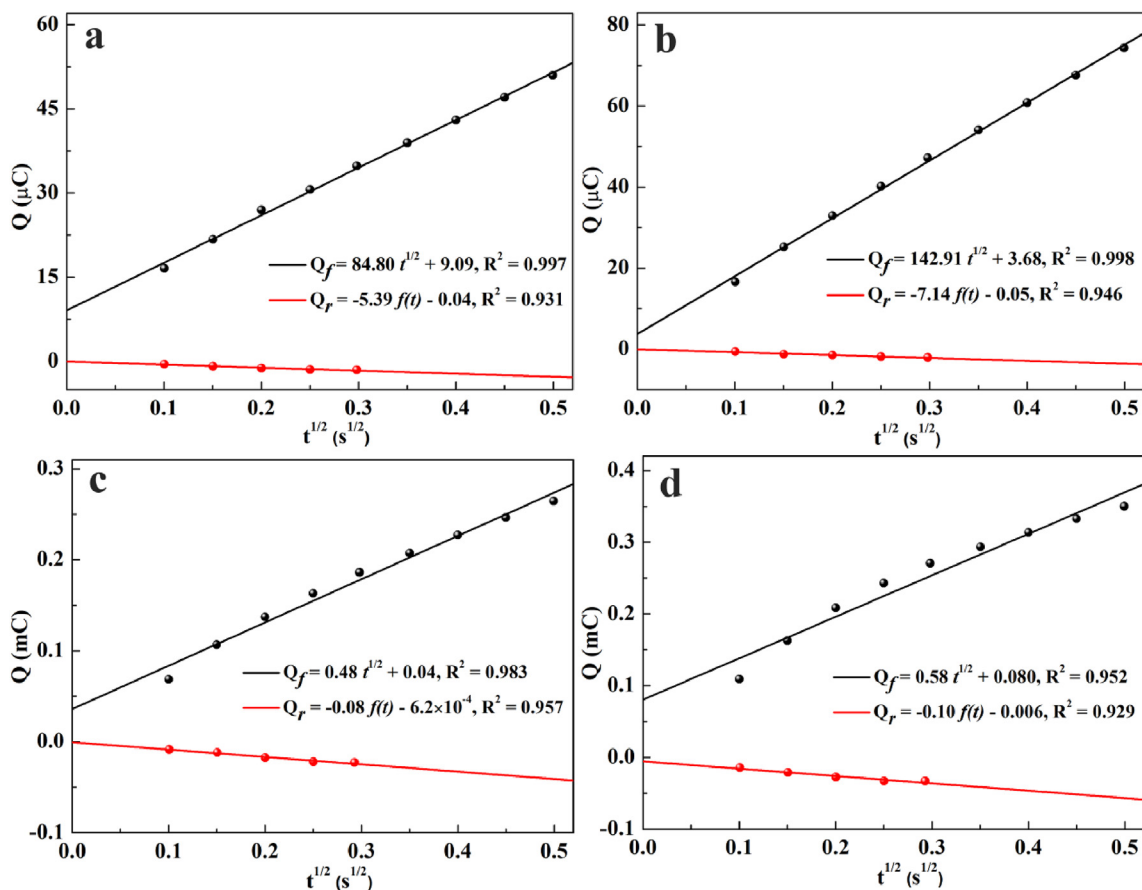

Fig. 6. Plots of Q$_f$ - $t^{1/2}$ during the forward step and Q$_r$ - $f(t)$ ($f(t) = \tau^{1/2} + (t - \tau)^{1/2} - t^{1/2}$, τ: the step time) during the reverse step in 0.1 M pH 9.0 PBS buffer solution of 50 μM hydroxylamine on (a) CCE, (b) HZIF-Mo/CCE, (c) PEDOT/CCE and (d) HZIF-Mo/PEDOT/CCE. The plus width is 0.25 s.

time of polymer is 60 min when the potential was applied for 0.70 V (Fig. S5a); the amperometric response drops as time goes on. The excess conductive polymer possibly hampers the diffusion of hydroxylamine on the layers between PEDOT and HZIF-Mo. When $0.03\ mg\ cm^{-2}$ of HZIF-Mo are immobilized in the CCEs, the obtained HZIF-Mo/PEDOT/CCE composites gives the relatively higher signal of hydroxylamine detection (Fig. S5c), possibly attributable to the weak conductivity of HZIF-Mo which hinders the electron transfer between HZIF-Mo layer and PEDOT. Further, as shown in amperometric responses about the voltage influence (Fig. S7c), the response signal of hydroxylamine is more pronounced when voltage set in the range from 0.65 to 0.80 V. Meanwhile, the intermediates or interferences generated at high potential (0.85 V) may concomitantly increase the noise signal, thus 0.80 V is selected as the working voltage.

3.2.3. Analytical performance of HZIF-Mo/PEDOT/CCE to hydroxylamine

Adopting the optimal detection conditions, hydroxylamine is detected using the available HZIF-Mo/PEDOT/CCE electrode by amperometric method (Fig. 7a); the corresponding calibration curve is shown in Fig. 7b, where different concentrations of hydroxylamine (from 0.1 up to 696.2 μM) is continuously injected to 0.1 M PBS (pH 9.0) buffer solution at +0.8 V. The high and rapid current response (within 5 s) denotes that the prepared sensor can timely capture the signal change of hydroxylamine. Accordingly, a linear plot of response current *versus* hydroxylamine concentration can be described as follows:

$$I(\mu A) = 3.03\ [hydroxylamine](\mu M) + 25.33$$

The detection limit (LOD) is approximately $0.04\ \mu M\ (S/N = 3)$ figured from the experimental results. Additionally, the HZIF-Mo/PEDOT/CCE sensor exhibits the favorable sensing performance of hydroxylamine detection comparison to other modified electrodes (Table S4).

The excellent performance of HZIF-Mo/PEDOT/CCE towards hydroxylamine detection probably attributes to the synergistic effect between HZIF-Mo and PEDOT: (i) the polyhedral HZIF-Mo skeleton has redox-active MoO_4 units (PXRD) along with high surface area and porosity (N_2 adsorption-desorption isotherm) [50]; (ii) PEDOT with the high conductivity (EIS) and mesoporous structure (N_2 adsorption-desorption isotherm) heightens the electronic transfer capacity. These synergies increase the amount of electroactive sites, electrochemically active surface and adsorption capacity, resulting in an enhancement in the competence of hydroxylamine detection.

3.2.4. Interference, stability and sample analysis

Selectivity and stability are important aspects for the practical application. Wherefore, the anti-interference measurement is performed in the presence of the potential interfering substance, including 100-fold concentrations of $H_2PO_4^-$, Br^-, SO_4^{2-}, HCO_3^-, CO_3^{2-}, Cl^-, CH_3COO^- and 2-fold concentrations of Pb^{2+}, Cd^{2+}, Hg^{2+}, Cu^{2+}, ClO_3^-, melamine, *o*-nitrophenol, *p*-nitrophenol, and ᴅ-fructose (Fig. S10). It is observed that the current response of HZIF-Mo/PEDOT/CCE towards hydroxylamine (25 μM) is almost no difference in the absence and presence of interfering substances, intimating that the sensor has splendid selectivity for hydroxylamine (Fig. 8a). Further, the electrochemical stability is recorded through
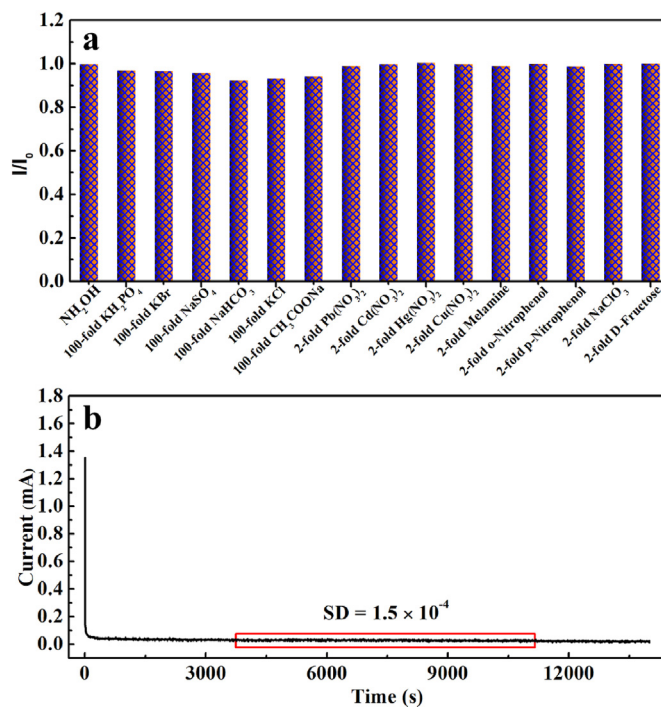
Fig. 8. (a) Interference measured by amperometric i-t test; I_0 and I stand the current of hydroxylamine in the absence and presence of interferents, respectively; (b) stability of chronoamperometry response to 0.2 mM hydroxylamine during 13,380 s.
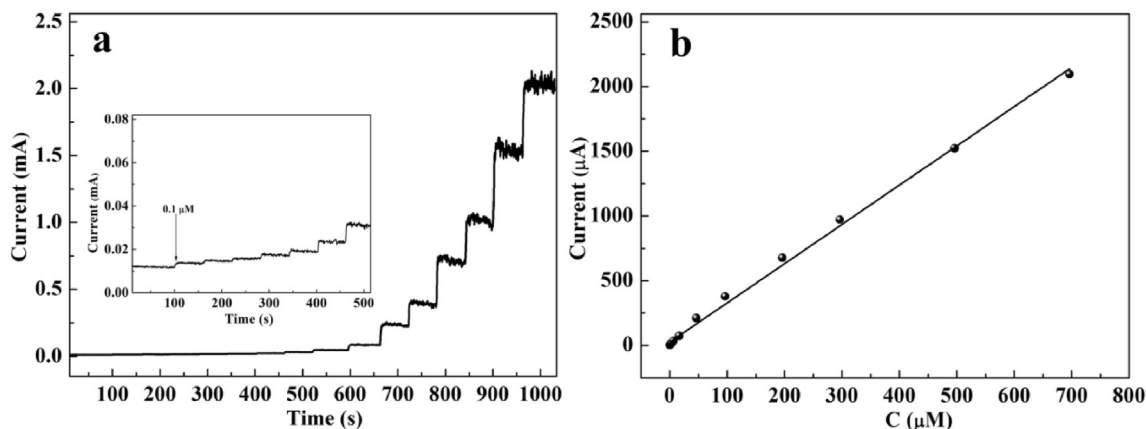
Fig. 7. (a) Amperometric curve of HZIF-Mo/PEDOT/CCE by stepwise injections of different hydroxylamine concentrations, and (b) the calibration curve of current response *versus* hydroxylamine concentration.
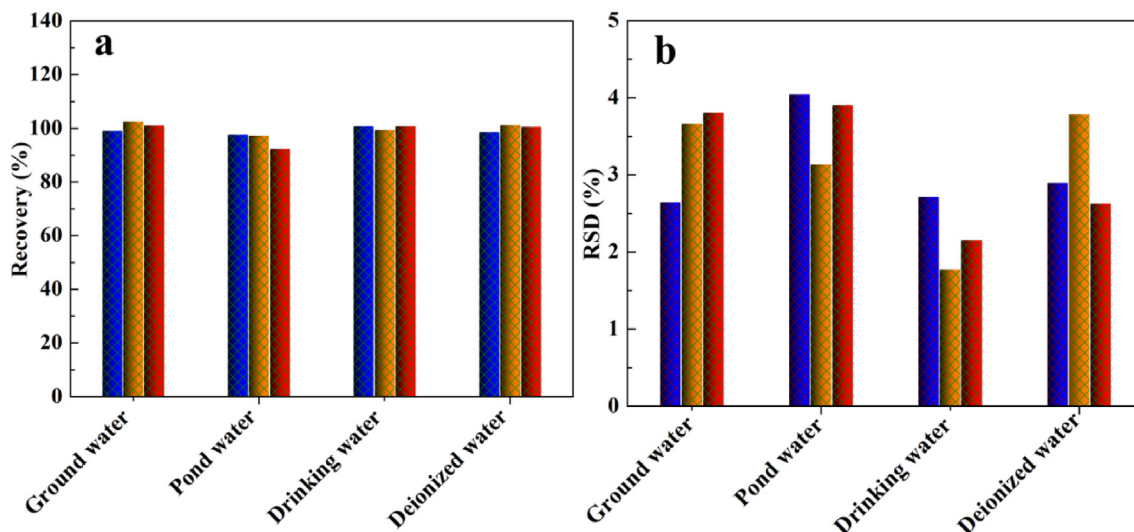
Fig. 9. (a) Recovery and (b) RSD (%) hydroxylamine from different water samples.

the chronoamperometric response to 0.2 mM hydroxylamine, as displayed in Fig. 8b. The variance (standard deviation $(SD) = 1.5 \times 10^{-4}$) between 3000 and 12,000 s implies that the degree of deviation is grand small and the stability is outstanding. The HZIF-Mo after hydroxylamine detection still retains in the electrode surface measured by SEM (Fig. S2f), and the characteristic PXRD patterns of HZIF-Mo also presents when the HZIF-Mo/PEDOT/CCE is immersed in PBS solution (pH 9.0) under ultrasonic conditions (40 kHz, KQ-100B, Kunshan, China) for 30 min (Fig. S6). Besides, amperometric currents of hydroxylamine on the five parallel electrodes are used to check reproducibility, and the relative standard deviation (RSD) is of 4.43% for 10 measurements.

The detective performance of HZIF-Mo/PEDOT/CCE towards the hydroxylamine in real samples such as pond water, drinking water, ground water, and single-deionized water are also analyzed by employing the standard method. All the real samples were straight invested for analysis after separately filtering. Upon adding the given quantity of hydroxylamine, the sample is measured for i-t method, and the results are outlined in Table S5 and Fig. 9. Notably, the recovery results are 92.62—102.80% that is satisfactory, and RSD is all less than 4.10%. Therefore, the HZIF-Mo/PEDOT/CCE sensor is reliable and sensitive to determine hydroxylamine in real samples.

4. Conclusions

In conclusion, HZIF-Mo/PEDOT/CCE composites are constructed and harnessed as novel sensors towards hydroxylamine detection. The hybrid sensor can immensely improve the signal currents, rooting in the synergistic effects from the inherent catalytic activity of HZIF-Mo and electrical conductivity of PEDOT. Thus, the HZIF-Mo/PEDOT/CCE sensor displayed a considerably low detection limit up to nanomolar levels (0.04 μM). More considerably, the sturdy and reproducible coating prompts a heightening in anti-interference ability and recovery in real samples. These absorbing electroanalytical performances facilitate this composite budding in practicable determination for chemical molecules.

Appendix A. Supplementary data

Supplementary data to this article can be found online at https://doi.org/10.1016/j.electacta.2019.134945.

References

[1] J. Li, S. Wang, S. Zou, H. Huang, Palladium-catalyzed relay hydro-aminocarbonylation of alkenes with hydroxylamine hydrochloride as an ammonia equivalent, Chem. Commun. 2 (2019) 14.

[2] L. Figueroa Cosme, Z.D. Hood, K.D. Gilroy, Y. Xia, A facile, robust and scalable method for the synthesis of Pd nanoplates with hydroxylamine as a reducing agent and mechanistic insights from kinetic analysis, J. Mater. Chem. C 6 (2018) 4677—4682.

[3] P. Gross, R.P. Smith, Biologic activity of hydroxylamine: a review, CRC Crit. Rev. Toxicol. 14 (1985) 87—99.

[4] P. Kumar, A. Deep, K.H. Kim, Metal organic frameworks for sensing applications, TrAC Trends Anal. Chem. (Reference Ed.) 73 (2015) 39—53.

[5] Q. Qiu, H. Chen, Y. Wang, Y. Ying, Recent advances in the rational synthesis and sensing applications of metal-organic framework biocomposites, Coord. Chem. Rev. 387 (2019) 60—78.

[6] A.J. Howarth, Y. Liu, P. Li, Z. Li, T.C. Wang, J.T. Hupp, O.K. Farha, Chemical, thermal and mechanical stabilities of metal−organic frameworks, Nat. Rev. Mater. 1 (2016) 15018.

[7] Y.V. Kaneti, S. Dutta, M.S. Hossain, M.J. Shiddiky, K.L. Tung, F.K. Shieh, C.K. Tsung, K.C.W. Wu, Y. Yamauchi, Strategies for improving the functionality of zeolitic imidazolate frameworks: tailoring nanoarchitectures for functional applications, Adv. Mater. 29 (2017) 1700213.

[8] T. Zhao, J. Gao, J. Wu, P. He, Y. Li, J. Yao, Highly active cobalt/tungsten carbide@ N-doped porous carbon nanomaterials derived from metal-organic frameworks as bifunctional catalysts for overall water splitting, Energy Technol. 7 (2019) 1800969.

[9] H. Zhang, Z. Ma, G. Liu, L. Shi, J. Tang, H. Pang, K. Wu, T. Takei, J. Zhang, Y. Yamauchi, J. Ye, Highly active nonprecious metal hydrogen evolution electrocatalyst: ultrafine molybdenum carbide nanoparticles embedded into a 3D nitrogen-implanted carbon matrix, NPG Asia Mater. 8 (2016) e293.

[10] Y.T. Xu, Z.M. Ye, J.W. Ye, L.M. Cao, R.K. Huang, J.X. Wu, D.D. Zhou, X.F. Zhang, C.T. He, J.P. Zhang, Non-3d metal modulation of a cobalt imidazolate framework for excellent electrocatalytic oxygen evolution in neutral media, Angew. Chem. 131 (2019) 145—149.

[11] X. Xu, H. Wang, J. Liu, H. Yan, The applications of zeolitic imidazolate framework-8 in electrical energy storage devices: a review, J. Mater. Sci. Mater. Electron. 28 (2017) 7532—7543.

[12] R.R. Salunkhe, Y.V. Kaneti, J. Kim, J.H. Kim, Y. Yamauchi, Nanoarchitectures for metal−organic framework-derived nanoporous carbons toward super-capacitor applications, Acc. Chem. Res. 49 (2016) 2796—2806.

[13] W. Zhang, L. zong, S. Liu, S. pei, Y. Zhang, X. Ding, B. Jiang, Y. Zhang, An electrochemical sensor based on electro-polymerization of caffeic acid and

Zn/Ni-ZIF-8−800 on glassy carbon electrode for the sensitive detection of acetaminophen, Biosens. Bioelectron. 131 (2019) 200−206.

[14] M. Hu, X. Hu, Y. Zhang, M. Teng, R. Deng, G. Xing, J. Tao, G. Xu, J. Chen, Y. Zhang, Label-free electrochemical immunosensor based on AuNPs/Zn/Ni-ZIF-8-800@ graphene composites for sensitive detection of monensin in milk, Sens. Actuators, B 288 (2019) 571−578.

[15] J. Qin, M.S. Cho, Y. Lee, Ferrocene encapsulated Zn zeolitic imidazole framework (ZIF-8) for optical and electrochemical sensing of amyloid-β oligomer and for the early diagnosis of Alzheimer's Disease, ACS Appl. Mater. Interfaces 11 (2019) 11743−11748.

[16] X. Chen, D. Liu, G. Cao, Y. Tang, C. Wu, In situ synthesis of sandwich-like graphene@ ZIF-67 heterostructure for highly sensitive nonenzymatic glucose sensing in human serums, ACS Appl. Mater. Interfaces 11 (2019) 9374−9384.

[17] C. Xiong, T. Zhang, W. Kong, Z. Zhang, H. Qu, W. Chen, Y. Wang, L. Luo, L. Zheng, ZIF-67 derived porous Co$_3$O$_4$ hollow nanopolyhedron functionalized solution-gated graphene transistors for simultaneous detection of glucose and uric acid in tears, Biosens. Bioelectron. 101 (2018) 21−28.

[18] W. Meng, Y. Wen, L. Dai, Z. He, L. Wang, A novel electrochemical sensor for glucose detection based on Ag@ ZIF-67 nanocomposite, Sens. Actuators, B 260 (2018) 852−860.

[19] A. Samadi Maybodi, S. Ghasemi, H. Ghaffari-Rad, A novel sensor based on Ag-loaded zeolitic imidazolate framework-8 nanocrystals for efficient electro-catalytic oxidation and trace level detection of hydrazine, Sens. Actuators, B 220 (2015) 627−633.

[20] L. Shi, X. Zhu, T. Liu, H. Zhao, M. Lan, Encapsulating Cu nanoparticles into metal-organic frameworks for nonenzymatic glucose sensing, Sens. Actuators, B 227 (2016) 583−590.

[21] Y. Wang, Y. Zhang, C. Hou, M. Liu, Magnetic Fe$_3$O$_4$@ MOFs decorated graphene nanocomposites as novel electrochemical sensor for ultrasensitive detection of dopamine, RSC Adv. 5 (2015) 98260−98268.

[22] Q. Yang, Q. Xu, S.H. Yu, H.L. Jiang, Pd nanocubes@ ZIF-8: integration of plasmon-driven photothermal conversion with a metal-organic framework for efficient and selective catalysis, Angew. Chem. Int. Ed. 55 (2016) 3685−3689.

[23] F. Wang, Z.S. Liu, H. Yang, Y.X. Tan, J. Zhang, Hybrid zeolitic imidazolate frameworks with catalytically active TO4 building blocks, Angew. Chem. Int. Ed. 50 (2011) 450−453.

[24] A. Sinha, Dhanjai, B. Tan, Y. Huang, H. Zhao, X. Dang, J. Chen, R. Jain, MoS$_2$ nanostructures for electrochemical sensing of multidisciplinary targets: a review, TrAC Trends Anal. Chem. (Reference Ed.) 102 (2018) 75−90.

[25] S. Hussain, S.A. Zaidi, D. Vikraman, H.S. Kim, J. Jung, Facile preparation of molybdenum carbide (Mo$_2$C) nanoparticles and its effective utilization in electrochemical sensing of folic acid via imprinting, Biosens. Bioelectron. (2019) 111330.

[26] T. Kokulnathan, T.W. Chen, S.M. Chen, J.V. Kumar, S. Sakthinathan, E.R. Nagarajan, Hydrothermal synthesis of silver molybdate/reduced graphene oxide hybrid composite: an efficient electrode material for the electrochemical detection of tryptophan in food and biological samples, Compos. B Eng. 169 (2019) 249−257.

[27] L. Liu, Y. Zhou, S. Liu, M. Xu, The applications of metal-organic frameworks in electrochemical sensors, ChemElectroChem 5 (2018) 6−19.

[28] J.M. D'Arcy, M.F. El Kady, P.P. Khine, L. Zhang, S.H. Lee, N.R. Davis, D.S. Liu, M.T. Yeung, S.Y. Kim, C.L. Turner, Vapor-phase polymerization of nanofibrillar poly (3, 4-ethylenedioxythiophene) for supercapacitors, ACS Nano 8 (2014) 1500−1510.

[29] S.P. Arnold, J.K. Harris, B. Neelamraju, M. Rudolph, E.L. Ratcliff, Microstructure-dependent electrochemical properties of chemical-vapor deposited poly (3, 4-ethylenedioxythiophene)(PEDOT) films, Synth. Met. 253 (2019) 26−33.

[30] H. Kang, M. Boyer, G.S. Hwang, J.w. Lee, Lithium-coated carbon cloth for anode of Lithium rechargeable batteries with enhanced cycling stability, Electrochim. Acta 303 (2019) 78−84.

[31] K.R. Reddy, H.M. Jeong, Y. Lee, A.V. Raghu, Synthesis of MWCNTs-core/thiophene polymer-sheath composite nanocables by a cationic surfactant-assisted chemical oxidative polymerization and their structural properties,

[32] A. Üğe, D. Koyuncu Zeybek, B. Zeybek, An electrochemical sensor for sensitive detection of dopamine based on MWCNTs/CeO$_2$-PEDOT composite, J. Electroanal. Chem. 813 (2018) 134−142.

[33] K.R. Reddy, W. Park, B.C. Sin, J. Noh, Y. Lee, Synthesis of electrically conductive and superparamagnetic monodispersed iron oxide-conjugated polymer composite nanoparticles by in situ chemical oxidative polymerization, J. Colloid Interface Sci. 335 (2009) 34−39.

[34] T. Abdiryim, A. Ubul, R. Jamal, F. Xu, A. Rahman, Electrochemical properties of the poly(3,4-ethylenedioxythiophene)/single-walled carbon nanotubes composite synthesized by solid-state heating method, Synth. Met. 162 (2012) 1604−1608.

[35] X. Han, T. Hu, Y. Wang, H. Chen, Y. Wang, R. Yao, X. Ma, J. Li, X. Li, A water-based mixing process for fabricating ZIF-8/PEG mixed matrix membranes with efficient desulfurization performance, Separ. Purif. Technol. 214 (2019) 61−66.

[36] R. Zamora, F. Masís-Meléndez, H. Phillips, L.A. Alvarado-Marchena, R. Starbird, Development of poly (3, 4-ethylenedioxythiophene (PEDOT)/carbon nanotube electrodes for electrochemical detection of mancozeb in water, Int. J. Electrochem. Sci. 13 (2018) 1931−1944.

[37] L. Gao, R. Yue, J. Xu, Z. Liu, J. Chai, Pt-PEDOT/rGO nanocomposites: one-pot preparation and superior electrochemical sensing performance for caffeic acid in tea, J. Electroanal. Chem. 816 (2018) 14−20.

[38] H.-J. Shin, S.S. Jeon, S.S. Im, CNT/PEDOT core/shell nanostructures as a counter electrode for dye-sensitized solar cells, Synth. Met. 161 (2011) 1284−1288.

[39] A.P. Sandoval-Rojas, M.T. Cortés, J. Hurtado, Electrochemical synthesis of poly(3,4-ethylenedioxythiophene) doped with a new bis(pyrazolyl)methane disulfonate and its behavior towards dopamine detection, J. Electroanal. Chem. 837 (2019) 200−207.

[40] Y. Xu, W. Lei, J. Su, J. Hu, X. Yu, T. Zhou, Y. Yang, D. Mandler, Q. Hao, A high-performance electrochemical sensor based on g-C$_3$N$_4$-E-PEDOT for the determination of acetaminophen, Electrochim. Acta 259 (2018) 994−1003.

[41] B. Sun, X. Gou, R. Bai, A.A.A. Abdelmoaty, Y. Ma, X. Zheng, F. Hu, Direct electrochemistry and electrocatalysis of lobetyolin via magnetic functionalized reduced graphene oxide film fabricated electrochemical sensor, Mater. Sci. Eng. C 74 (2017) 515−524.

[42] M.M. Foroughi, H. Beitollahi, S. Tajik, M. Hamzavi, H. Parvan, Hydroxylamine electrochemical sensor based on a modified carbon nanotube paste electrode: application to determination of hydroxylamine in water samples, Int. J. Electrochem. Sci 9 (2014) 2955−2965.

[43] S. Tajik, H. Mahmoudi-Moghaddam, H. Beitollahi, Screen-printed electrode modified with La^{3+}-doped Co$_3$O$_4$ nanocubes for electrochemical determination of hydroxylamine, J. Electrochem. Soc. 166 (2019) B402−B406.

[44] Y. Wang, L. Wang, H. Chen, X. Hu, S. Ma, Fabrication of highly sensitive and stable hydroxylamine electrochemical sensor based on gold nanoparticles and metal−metalloporphyrin framework modified electrode, ACS Appl. Mater. Interfaces 8 (2016) 18173−18181.

[45] Y.J. Yang, W. Li, Gold nanoparticles/graphene oxide composite for electrochemical sensing of hydroxylamine and hydrogen peroxide, Fullerenes, Nanotub. Carbon Nanostruct. 26 (2018) 195−204.

[46] F. Anson, Application of potentiostatic current integration to the study of the adsorption of cobalt (III)-(Ethylenedinitrilo (tetraacetate) on mercury electrodes, Anal. Chem. 36 (1964) 932−934.

[47] F.C. Anson, Innovations in the study of adsorbed reactants by chronocoulometry, Anal. Chem. 38 (1966) 54−57.

[48] E.G. Pineda, M.J.R. Presa, C.A. Gervasi, A.E. Bolzán, Tubular-structured polypyrrole electrodes decorated with gold nanoparticles for electrochemical sensing, J. Electroanal. Chem. 812 (2018) 28−36.

[49] J. Li, X. Lin, Electrocatalytic oxidation of hydrazine and hydroxylamine at gold nanoparticle-polypyrrole nanowire modified glassy carbon electrode, Sens. Actuators, B 126 (2007) 527−535.

[50] S. Kempahanumakkagari, K. Vellingiri, A. Deep, E.E. Kwon, N. Bolan, K.H. Kim, Metal−organic framework composites as electrocatalysts for electrochemical sensing applications, Coord. Chem. Rev. 357 (2018) 105−129.